

# Measurement of the Beam Asymmetry $\Sigma$ in the Forward Direction for $\vec{\gamma}p \rightarrow p\pi^0$

N. Sparks,<sup>1</sup> V. Crede,<sup>1</sup> A.V. Anisovich,<sup>2,3</sup> J.C.S. Bacelar,<sup>4</sup> R. Bantes,<sup>2</sup> O. Bartholomy,<sup>2</sup> D. Bayadilov,<sup>2,3</sup>  
 R. Beck,<sup>2</sup> Y.A. Beloglazov,<sup>3</sup> R. Castelijns,<sup>4</sup> D. Elsner,<sup>5</sup> R. Ewald,<sup>5</sup> F. Frommberger,<sup>5</sup> Chr. Funke,<sup>2</sup>  
 R. Gregor,<sup>6</sup> A. Gridnev,<sup>3</sup> E. Gutz,<sup>2</sup> W. Hillert,<sup>5</sup> P. Hoffmeister,<sup>2</sup> I. Jaegle,<sup>7</sup> J. Junkersfeld,<sup>2</sup> H. Kalinowsky,<sup>2</sup>  
 S. Kammer,<sup>5</sup> Frank Klein,<sup>5</sup> Friedrich Klein,<sup>5</sup> E. Klempt,<sup>2</sup> M. Kotulla,<sup>7,6</sup> B. Krusche,<sup>7</sup> H. Löhner,<sup>4</sup>  
 I.V. Lopatin,<sup>3</sup> S. Lugert,<sup>6</sup> D. Menze,<sup>5</sup> T. Mertens,<sup>7</sup> J.G. Messchendorp,<sup>4,6</sup> V. Metag,<sup>6</sup> M. Nanova,<sup>6</sup>  
 V.A. Nikonov,<sup>2,3</sup> D. Novinski,<sup>3</sup> R. Novotny,<sup>6</sup> M. Ostrick,<sup>5</sup> L.M. Pant,<sup>6</sup> H. van Pee,<sup>2</sup> M. Pfeiffer,<sup>6</sup> A. Roy,<sup>6</sup>  
 A.V. Sarantsev,<sup>2,3</sup> S. Schadmand,<sup>8</sup> C. Schmidt,<sup>2</sup> H. Schmieden,<sup>5</sup> B. Schoch,<sup>5</sup> S. Shende,<sup>4</sup> V. Sokhoyan,<sup>2</sup> A. Stüle,<sup>5</sup>  
 V.V. Sumachev,<sup>3</sup> T. Szczepanek,<sup>2</sup> U. Thoma,<sup>2</sup> D. Trnka,<sup>6</sup> R. Varma,<sup>6</sup> D. Walther,<sup>2,5</sup> Ch. Wendel,<sup>2</sup> and A. Wilson<sup>1</sup>

(The CBELSA/TAPS Collaboration)

<sup>1</sup>*Department of Physics, Florida State University, Tallahassee, Florida 32306, USA*

<sup>2</sup>*Helmholtz-Institut für Strahlen- und Kernphysik, Universität Bonn, D-53115 Bonn, Germany*

<sup>3</sup>*Petersburg Nuclear Physics Institute, RU-188350 Gatchina, Russia*

<sup>4</sup>*KVI, 9747 AA Groningen, The Netherlands*

<sup>5</sup>*Physikalisches Institut, Universität Bonn, D-53115 Bonn, Germany*

<sup>6</sup>*II. Physikalisches Institut, Universität Gießen, D-35392 Gießen, Germany*

<sup>7</sup>*Physikalisches Institut, Universität Basel, CH-4056 Basel, Switzerland*

<sup>8</sup>*Institut für Kernphysik, Forschungszentrum Jülich, D-52428 Jülich, Germany*

(Dated: Received: September 5, 2018/ Revised version:)

Photoproduction of neutral pions has been studied with the CBELSA/TAPS detector for photon energies between 0.92 and 1.68 GeV at the electron accelerator ELSA. The beam asymmetry  $\Sigma$  has been extracted for  $115^\circ < \theta_{\text{c.m.}} < 155^\circ$  of the  $\pi^0$  meson and for  $\theta_{\text{c.m.}} < 60^\circ$ . The new beam asymmetry data improve the world database for photon energies above 1.5 GeV and, by covering the very forward region, extend previously published data for the same reaction by our collaboration. The angular dependence of  $\Sigma$  shows overall good agreement with the SAID parameterization.

PACS numbers: 13.60.Le Meson production, 13.60.-r Photon and charged-lepton interactions with hadrons, 13.75.Gx Pion-baryon interactions, 13.88.+e Polarization in interactions and scattering, 14.40.Aq  $\pi$ ,  $K$ , and  $\eta$  mesons, 25.20.Lj Photoproduction reactions

## I. INTRODUCTION

Baryon resonances exhibit a rich excitation spectrum due to their complicated substructure. The understanding of this structure of the nucleon and its excited states is one of the key questions in hadronic physics. Although most quark models based on three constituent quark degrees of freedom can describe ground-state baryons well, they fail in some important details. Known as the missing-resonance problem, these quark models have predicted many more excited states at and above 2 GeV/ $c^2$  than have been found experimentally. Of particular importance are the measurements of polarization observables in addition to the extraction of total and differential cross sections. These polarization observables can be sensitive to interference terms in the theoretical interpretation of the data and, thus, can provide access to otherwise small resonance contributions. The beam asymmetry  $\Sigma$ , for example, which arises from a linearly polarized photon beam, addresses the non-spin-flip terms in the transition current (e.g., convection currents and double spin-flip contributions), whereas spin-flip contributions are projected out by a circularly polarized photon beam.

Since the  $\pi$  meson has isospin  $I = 1$ , both nucleon resonances ( $I = 1/2$ ) and  $\Delta$  resonances ( $I = 3/2$ ) can con-

tribute to  $\pi^0$  photoproduction off the proton. The total  $\pi^0$  cross section exhibits three clear peaks and a broad enhancement around  $W \approx 1900$  MeV/ $c^2$ , which represent the four known resonance regions below 2 GeV/ $c^2$ . The first resonance region below 1500 MeV/ $c^2$  is dominated by the well-known  $\Delta(1232)P_{33}$  resonance with very small contributions of the  $N(1440)P_{11}$  Roper resonance. The  $N(1520)D_{13}$  and the two  $S_{11}$  resonances combined,  $N(1535)S_{11}$  and  $N(1650)S_{11}$ , contribute with about equal strength to the second resonance region around 1550 MeV/ $c^2$ . The third bump in the  $p\pi^0$  total cross section is mainly due to three major resonance contributions:  $\Delta(1700)D_{33}$ ,  $N(1680)F_{15}$ , and  $N(1650)S_{11}$  (e.g., Refs. [1–3]). In the less known fourth resonance region, the two well-established  $\Delta$  excitations  $\Delta(1950)F_{37}$  and  $\Delta(1920)P_{33}$  have been found to contribute (e.g., Ref. [1]). The inclusion of polarization observables as additional constraints in the analysis of  $\pi^0$  photoproduction data will not only help reveal contributions of resonances that couple only weakly to the  $\pi^0$ , but will also help to better understand the properties of these well-established resonances (e.g., the structure of the transition current).

In this paper, we present the beam asymmetry  $\Sigma$  for the reaction:

$$\vec{\gamma}p \rightarrow p\pi^0, \quad \text{where } \pi^0 \rightarrow 2\gamma. \quad (1)$$

The polarization data cover an incoming photon energy

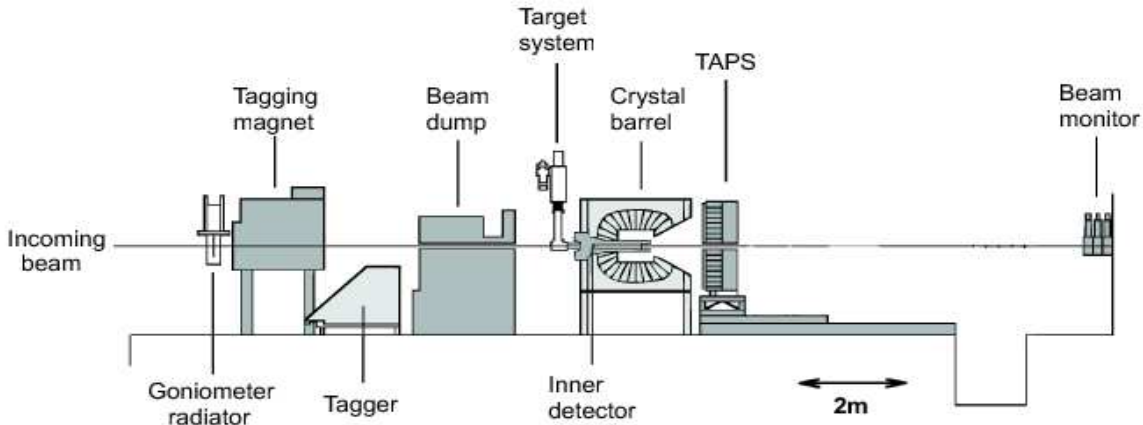


FIG. 1: Experimental setup of CBELSA/TAPS in Bonn. The electron beam delivered by the accelerator ELSA enters from the left side and hits the diamond crystal of the goniometer in front of the tagger magnet.

range between about 920 and 1680 MeV and, in addition to  $115^\circ < \theta_{c.m.} < 155^\circ$ , the most forward angular range of the  $\pi^0$  meson  $\theta_{c.m.} < 60^\circ$ .

The paper has the following structure. Section II summarizes the data that were published before this analysis. An introduction to the CBELSA/TAPS experimental setup is given in Sec. III. The data reconstruction and selection are discussed in Sec. IV, and the extraction of beam asymmetries is described in Sec. V. Experimental results are finally presented in Sec. VI.

## II. PREVIOUS RESULTS

Cross section data for  $\pi^0$  photoproduction were obtained and studied at many different laboratories over a wide kinematic range [4–17]. A review of the main data sets and a corresponding comparison of their coverage in energy and solid angle can be found in Ref. [15].

Polarization observables for single- $\pi^0$  photoproduction have been determined mostly by using a linearly polarized beam [11, 12, 14, 17, 19–26]. In the following, a summary is given of the experiments performed after 1970 that allowed the extraction of the beam asymmetry  $\Sigma$ . Most of the experiments accumulated data at very low energies ( $< 500$  MeV); only very recently have data been taken above 1 GeV in the incoming photon energy.

In the 1970s, one of the earlier experiments used linearly polarized photons with energies from 610 to 940 MeV. The experiments were carried out by using the backscattered laser beam and the 82-in. bubble chamber at SLAC [19]. At the Cambridge Electron Accelerator, beam asymmetries and cross sections at  $\theta_{c.m.} = 90^\circ$  were measured with photon energies that ranged from 0.8 to 2.2 GeV [20]. Finally, the Daresbury synchrotron allowed a study of the photon asymmetry over a range of photon energies from 1.2 to 2.8 GeV and over a range of  $-t$  from 0.13 to 1.4  $(\text{GeV}/c)^2$  [21, 22].

Belyaev *et al.* measured  $\Sigma$  in addition to the target asymmetry  $T$  and the double-polarization observable  $P$  by using linearly polarized photons and a transversely polarized proton target. The measurements were made in the energy range  $E_\gamma \in [280, 450]$  MeV and at  $\pi^0$  c.m. angles between  $60^\circ$  and  $135^\circ$  [23].

Beck *et al.* measured differential cross sections at the electron accelerator MAMI (Mainz Microtron) between the threshold at 144 MeV up to photon energies of 157 MeV [7] as well as for energies between 270 and 420 MeV [8]. Both experiments used a linearly polarized photon beam produced via coherent bremsstrahlung. In Ref. [8],  $\pi^0$  photoproduction was studied with the DAPHNE detector, which covered  $\sim 94\%$  of the solid angle.

In another experiment at MAMI, Schmidt *et al.* measured the photon asymmetry between threshold and 166 MeV by using the photon spectrometer TAPS. Total and differential cross sections were extracted simultaneously and were compared to predictions of chiral perturbation theory and low-energy theorems [11].

Blanpied *et al.* extracted unpolarized differential cross sections and beam asymmetry angular distributions at BNL by using LEGS for photon beam energies in the range from 213 to 333 MeV [12, 24]. Final-state particles were detected in an array of six NaI crystals.

The Erevan group published data from several experiments. More recently, Adamian *et al.* extracted asymmetry data in the energy range 500–1000 MeV and for  $\pi^0$  angles between  $85^\circ$  and  $125^\circ$  with energy and angle steps of 25 MeV and  $5^\circ$ , respectively [25].

More recently, the GRAAL collaboration at ESRF in Grenoble extracted  $\Sigma$  over a wide angular range, although limited to  $\cos\theta_{c.m.} < 0.7$ . The data cover incoming photon energies between 550 and 1475 MeV [14]. At GRAAL, Compton backscattering of low-energy photons off ultrarelativistic electrons reached almost 100% beam polarization at the Compton edge.

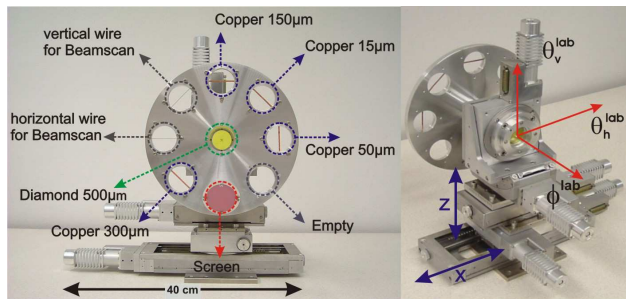


FIG. 2: (Color online) Photograph of the goniometer setup for the CBELSA/TAPS experiment; picture taken from Ref. [26].

The LEPS collaboration at SPring-8 in Hyogo, Japan, measured beam asymmetries for higher photon energies between  $E_\gamma = 1500$  and  $2400$  MeV and, for the first time, at  $\pi^0$  backward angles  $-1 < \cos\theta_{c.m.} < -0.6$  [17]. Backward-Compton scattering was applied by using Ar-ion laser photons with a 351-nm wavelength.

Recent CBELSA/TAPS asymmetry data cover photon energies between 760 and 1400 MeV and an angular range mostly in the backward direction of the  $\pi^0$  meson ( $110^\circ < \theta_{c.m.} < 160^\circ$ ). For most of the energy bins, additional data points can be found in the angular region  $50^\circ < \theta_{c.m.} < 60^\circ$ ; there are a few data points at about  $\theta_{c.m.} = 40^\circ$  [26].

### III. EXPERIMENTAL SETUP

The results presented here are partially based on a reanalysis of the data discussed in Ref. [26]. The experiment was carried out at the electron accelerator facility ELSA [27] at the University of Bonn, Germany, by using a combination of the Crystal Barrel [28] and TAPS [29, 30] calorimeters. A schematic of the experimental setup at the ELSA facility is shown in Fig. 1.

Electrons with an energy of  $E_0 = 3.175$  GeV were extracted from ELSA via slow (resonant) extraction. The electron beam then hit the radiator target positioned in front of the tagging magnet. The goniometer setup and its performance is fully described in Refs. [26, 31]. Since the development of the hardware and the production of linearly polarized photons is not part of the analysis presented here, only a very brief description of the setup is given. Several amorphous copper radiators with different radiation lengths surrounded the diamond crystal (Fig. 2). The crystal measured  $500 \mu\text{m}$  in thickness and had a front surface of  $4 \times 4$  mm; it was glued to a  $12.5 \mu\text{m}$  kapton foil and was accurately positioned by a dedicated commercial five-axis goniometer. A wobble along the axes limited the maximum angular uncertainty to  $\delta < 170 \mu\text{rad}$ . All other uncertainties were negligible.

The electrons undergoing the bremsstrahlung process were deflected in the dipole magnet according to their en-

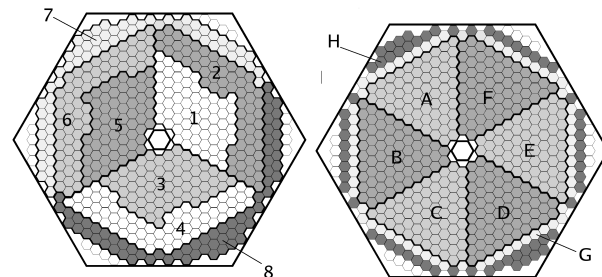
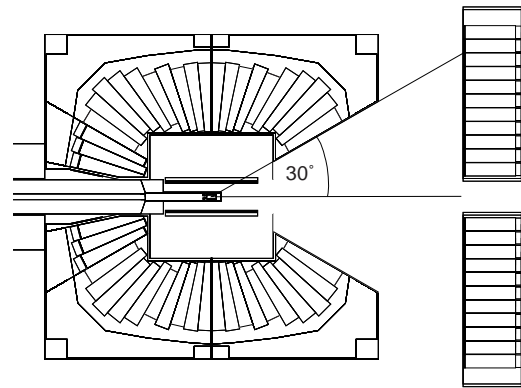


FIG. 3: Top: Schematic of the liquid-hydrogen target, scintillating-fiber detector, Crystal Barrel and TAPS calorimeters. Bottom: Front view of TAPS; the left side shows the logical segmentation for the LED-low trigger, the right side the logical segmentation for the LED-high trigger (see text for more details).

ergy loss; the remaining energy was determined in a tagging detector consisting of 480 scintillating fibers above 14 scintillation counters in a configuration with adjacent paddles partially overlapping. The corresponding energy of an emitted photon was  $E_\gamma = E_0 - E_{e^-}$ . Electrons not undergoing bremsstrahlung were deflected at small angles and were guided into a beam dump located behind the tagger detectors. The energy resolution is about 2 MeV for the high-energy photons and 25 MeV for the low-energy part of the bremsstrahlung spectrum.

For the energy calibration of the tagging system, a polynomial was determined in simulations using the measured field map of the bending magnet and the known positions of the fibers. The calibration was then cross-checked by measurements with the ELSA electron beam at two different energies. At 600 and 800 MeV, a low-current beam was guided directly into the tagger, while the magnetic field was slowly varied. More details of the calibration can be found in Ref. [32].

The photons hit the liquid-hydrogen target in the center of the Crystal Barrel (CB) calorimeter. The target cell (5 cm in length, 3 cm in diameter) was surrounded by a scintillating-fiber detector [33], which provided an unambiguous impact point for charged particles (due to the arrangement of its three layers) leaving the target.

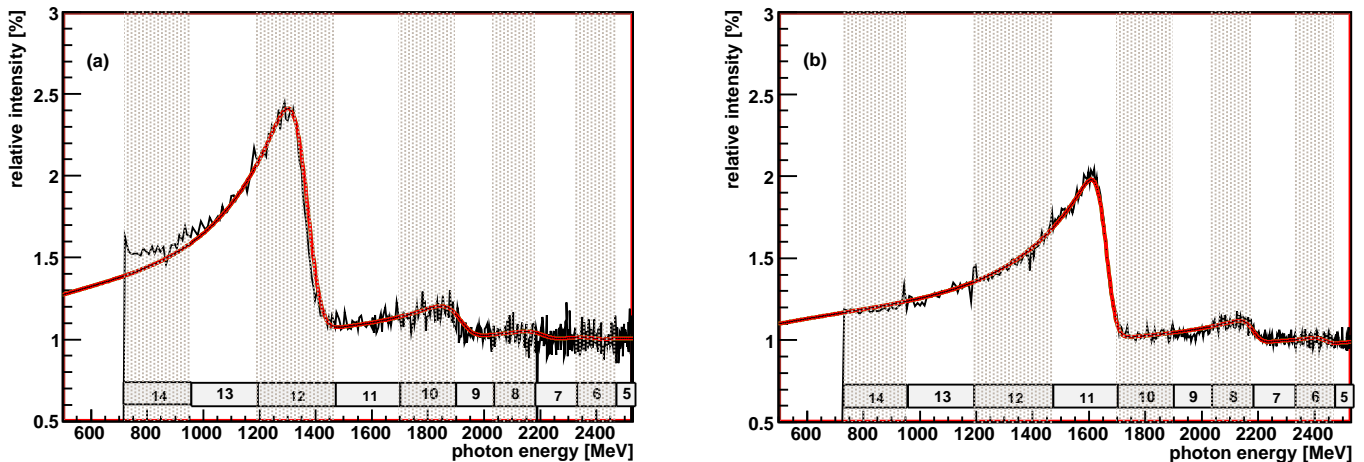


FIG. 4: (Color online) The measured coherent bremsstrahlung intensities normalized to an incoherent spectrum [26]. The full curve shows how well the data are described by the model calculations [31]. For this experiment, the diamond radiator was oriented such that intensity maxima at (a)  $E_\gamma = 1305$  MeV and (b)  $E_\gamma = 1610$  MeV were reached. The boxes at the bottom of each distribution indicate the ranges covered by the 14 scintillation counters of the tagger.

The CB calorimeter in its CBELSA/TAPS configuration of 2002–2003 consisted of 1290 CsI(Tl) crystals with a length of  $16 X_R$ . The modules have an excellent photon detection efficiency; a detailed description can be found in Ref. [28]. For this series of experiments, the (downstream) rings 11–13 were removed to combine the detector with TAPS in the forward direction. The CB calorimeter covered the complete azimuthal angle and polar angles from  $30^\circ$  to  $168^\circ$ . All crystals are of trapezoidal shape pointing to the center of the target (Fig. 3, top).

The TAPS detector consisted of 528 hexagonal  $\text{BaF}_2$  crystals with a length of about  $12 X_R$ . It was configured as a hexagonal wall serving as the forward end cap of the CB calorimeter (Fig. 3, bottom). TAPS provided a high granularity in the forward direction for polar angles between  $5^\circ$  and  $30^\circ$  (full  $\phi$  coverage). A 5-mm thick plastic scintillator in front of each TAPS module allowed the identification of charged particles. The combination of the CB and TAPS calorimeters covered 99% of the  $4\pi$  solid angle and served as an excellent setup to detect multiphoton final states.

The fast response of the TAPS modules provided the first-level trigger. The second-level trigger was based on a cellular logic (FACE), which determined the number of clusters in the barrel. The trigger required either two hits above a low-energy threshold in TAPS (LED-low) or one hit above a higher-energy threshold in TAPS (LED-high) in combination with at least two FACE clusters. The shape of the logical segmentation for the TAPS trigger is shown in Fig. 3 (bottom).

### A. Linearly polarized photons

Two methods are usually applied for preparing a linearly polarized photon beam: coherent bremsstrahlung

and Compton backscattering. In the latter technique, linearly polarized laser photons are backscattered off a high-energy electron beam (e.g., Refs. [14, 34]). The degree of polarization that can be achieved by using this technique is proportional to that of the initial laser beam. Although high degrees of polarization can, in principle, be reached, the photon beam intensities are usually lower than those from coherent bremsstrahlung because of limitations resulting from the operation of a multiuser storage ring. In contrast, many facilities have successfully produced linearly polarized beams by using coherent electron bremsstrahlung [26, 35], where the recoil momentum of the recoiling nucleus embedded in the crystal is transferred to the crystal lattice. For the CBELSA/TAPS experiment, a diamond crystal was used. For certain orientations of this diamond, the recoil momentum can be entirely transferred to the crystal; this defines the deflection plane of the electrons and results in a strong linear polarization of the photon beam.

For the beam asymmetry data presented in this paper, the crystal alignment was achieved by the so-called *Stonehenge Technique* [36]. An overview of the alignment process for the CBELSA/TAPS goniometer, which includes a brief description of the Stonehenge Technique, is given in Ref. [26]. The stability of the beam position was monitored online to preserve the alignment during the experiment. The coherent peak itself was used for this procedure because the position of the coherent edge in the energy spectrum is extremely sensitive to the angle of the incident beam [32].

The degree of linear polarization was determined in Ref. [31] by comparing the measured photon spectrum with a model calculation using the ANB (analytic bremsstrahlung calculation) software [37]. Fig. 4 shows photon intensity spectra normalized to incoherent spectra [26] for the two different positions of the coherent edge used in this analysis. The curves represent calcula-

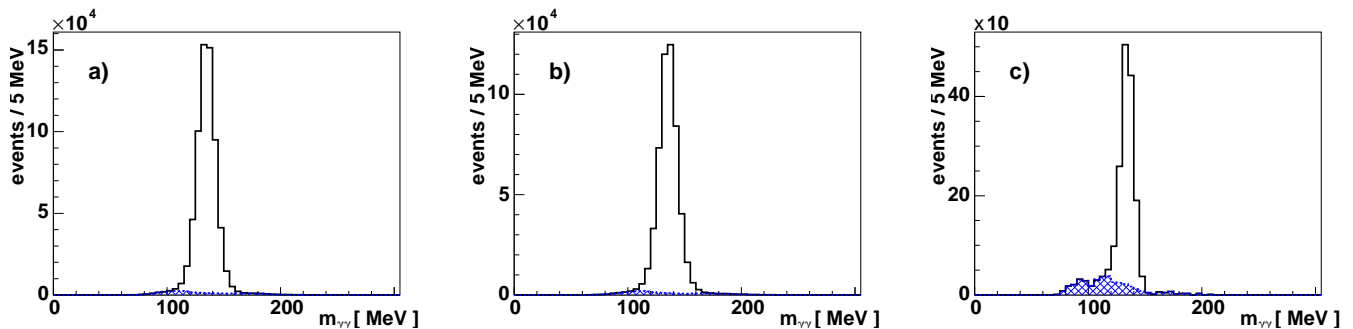


FIG. 5: (Color online) Invariant  $\gamma\gamma$ -mass spectra for the reaction  $\gamma p \rightarrow p\gamma\gamma$  using data with the coherent peak at 1305 MeV (left) and at 1610 MeV (center); confidence level cuts were applied at  $10^{-2}$ . The  $\pi^0$  mesons are observed with very little background. On the right, a mass spectrum for a forward bin is shown at  $E_\gamma = 1097$  MeV (bin width 33 MeV) and  $\theta_{c.m.} = 25^\circ \pm 5^\circ$ . The colored area (bottom) indicates the background (for the background determination, see Sec. IV B).

tions by using an improved version of the original ANB code [31], which takes the effects of beam divergence, beam spot size, energy resolution, and multiple scattering into account. The description of the measured spectra is excellent at all energies and coherent peak positions. An absolute error of  $\delta P_\gamma < 0.02$  is estimated by using variations of the calculated relative intensity by  $\pm 5\%$  [26]. These worst-case estimates account for deviations from the shape of the spectrum caused by combined statistical and systematic effects.

#### IV. PREPARATION OF FINAL STATE

The data presented here were accumulated in March and May of 2003 in two run periods with an ELSA beam energy of 3.175 GeV. Events for coherent peak positions at 1305 and 1610 MeV were recorded. These CBELSA/TAPS polarization data were used to extract the beam asymmetries for a large variety of photoproduction reactions [26, 38–41]. The analysis discussed here, for the peak position at 1305 MeV, is partially a reanalysis of the data published in Ref. [26]. The event reconstruction and selection of the  $\pi^0$  channel for Reaction (1) is presented in this section. A total number of  $\sim 1.06 \times 10^6$   $\pi^0$  events has been included in this analysis.

##### A. Event reconstruction

Events with two or three (neutral or charged) particles in the final state were selected. The experimental setup allows the identification of charged clusters in TAPS by using the plastic scintillators mounted in front of each BaF<sub>2</sub> crystal. The efficiencies of these (photon)-veto detectors were determined and were modeled in the Monte Carlo program. Although these detectors have been used in a recent extraction of unpolarized  $\eta$  and  $\eta'$  differential cross sections [42], we decided not to employ this information in the analysis to avoid a possible  $\phi$  dependence of the data on these detector components. Instead, the

proton in all events with three particles was identified by successively assigning the proton tag to each final-state particle (and by assuming the remaining two particles are photons) and then by testing the hypothesis  $\gamma p \rightarrow p\gamma\gamma$  in a 1C kinematic fit only requiring energy and momentum conservations. Simultaneously, all possible tagger photons were tested. A prompt coincidence within  $-5$  to  $+15$  ns between a particle in TAPS and an electron in the tagger was required to reduce time-accidental background. The best fit based on its  $\chi^2$  probability or confidence level (CL) defined the proton as well as the initial photon and its corresponding energy.

On average, proton clusters in the calorimeters are much smaller than photon clusters and can sometimes consist of only one or two crystals; this provides an insufficient resolution. For this reason, proton identification was used only to remove the proton from the list of final-state particles. The proton momentum was then reconstructed from the event kinematics in “missing-proton” kinematic fitting.

The use of kinematic fitting in CBELSA/TAPS data analyses has been described in more detail in Ref. [42]. In this analysis, all events were subject to the hypothesis:

$$\gamma p \rightarrow p n_\gamma \gamma, \quad (2)$$

which simply imposes energy and momentum conservations without a  $\pi^0$  mass constraint. Figure 5 shows the remaining invariant  $\gamma\gamma$  mass for all events satisfying Eq. (2) at a CL  $> 10^{-2}$ . A clear peak for the  $\pi^0$  meson is visible. The background underneath the peak was subtracted for every  $(E_\gamma, \theta_{c.m.}, \phi)$  bin by using the so-called Q-factor method described in the following section.

##### B. Background subtraction

Mass distributions for  $(E_\gamma, \theta_{c.m.}, \phi)$  bins in the forward direction of the  $\pi^0$  meson show some residual background under the meson peak. The separation of background events from signal events is typically done by using the

side-band subtraction method. In this approach, events from outside the signal region are subtracted from those inside the signal region to remove the background from the distribution.

We decided to use an event-based approach called the  $Q$ -factor method, which assigns a signal probability  $Q_i$  to each event. The approach is described in detail in Ref. [43]. In most of our forward bins, the functional form of the background shape  $B(m, \vec{\xi})$  is unknown, where each  $\gamma p \rightarrow p\gamma\gamma$  event has kinematic variables  $\vec{\xi} = (E_\gamma, \cos\theta_{\text{c.m.}}^{\gamma\gamma}, \phi_{\gamma\gamma}, M_{\gamma\gamma}, \phi^*, \theta^*)$ . The two variables  $\phi^*$  and  $\theta^*$  denote the azimuthal and polar angles in the rest frame of the two photons; these angles are measured with respect to the coordinate system formed by the unit vector  $\hat{z}'$  in the direction of the two-photon system in the c.m. frame, the unit normal  $\hat{y}'$  to the reaction plane (defined below), and  $\hat{x}' = \hat{y}' \times \hat{z}'$ . The azimuthal angle  $\phi^*$  is also given by the angle between the reaction plane and the two-photon decay plane, where the reaction plane is spanned by the beam axis and the recoiling proton (or the two-photon system); both of these planes are formed by particles in the c.m. system. The invariant  $\gamma\gamma$  mass was chosen as the reference variable for which the background dependence was studied. The distance between any two events in the space spanned by  $\vec{\xi}$  is given by [43]

$$d_{ij}^2 = \sum_{k=1}^6 \left[ \frac{\xi_k^i - \xi_k^j}{r_k} \right]^2, \quad (3)$$

where  $r_k$  denotes the range of  $\xi_k$  and the reference variable is excluded in the sum. We then found the closest 100 events for each event  $i$ , with kinematics  $\vec{\xi}_i$  and  $\gamma\gamma$  mass  $M_i$ , according to Eq. (3). Since these 100 events occupy a very small region around  $\vec{\xi}_i$ , a linear approximation is validated for the mass dependence of the background. A Gaussian line shape was used to model the  $\pi^0$  signal. We have used the unbinned maximum likelihood method to obtain the parameters describing the mass distributions. By using these fit results, the expected number of signal and background events, denoted as  $s_i$  and  $b_i$ , respectively, can be calculated at  $M_i$  and for each event, the  $Q$ -factor can be written as

$$Q_i = \frac{s_i}{s_i + b_i}, \quad \text{where } N_{\text{signal}} = \sum_i^N Q_i. \quad (4)$$

This method delivered a reliable subtraction of the background from our mass distributions. The background visible in Fig. 5 has been determined using this method. The  $Q$ -factor errors (or systematic uncertainties on signal-yield extractions) contribute strongly to the total systematic uncertainty of the extracted polarization observables. A full discussion of the error estimation and event correlations goes beyond the scope of this paper and can be found in Ref. [43].

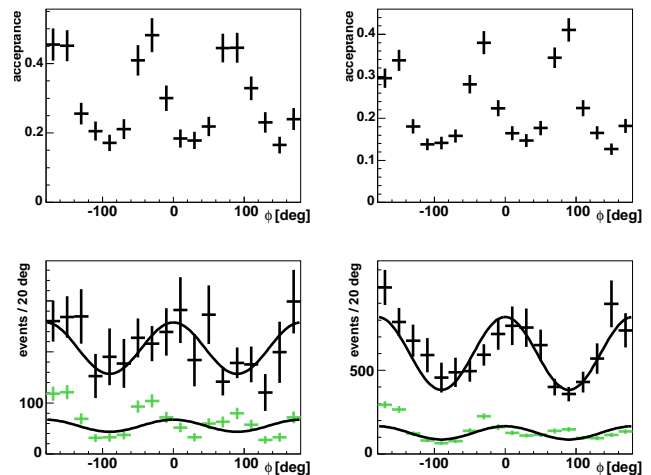


FIG. 6: (Color online) Influence of the hardware trigger. The top row shows the acceptance for  $E_\gamma \sim 1560$  MeV as well as  $\theta_{\text{c.m.}} = 15^\circ \pm 5^\circ$  (left) and  $\theta_{\text{c.m.}} = 25^\circ \pm 5^\circ$  (right), respectively. The three-peak structure between the trigger segments is visible (see text for more details). The corresponding data  $\phi$  distributions are given in the bottom row. The colored distributions (bottom) show the uncorrected distributions and the black data points (top) show the acceptance-corrected data. The improvement can clearly be observed.

### C. Monte Carlo simulations

The performance of the detector was simulated in GEANT3-based Monte Carlo studies. We used a program package that was built upon a program developed for the CB-ELSA experiment. The Monte Carlo program accurately reproduces the response of the TAPS and CB crystals when hit by a photon.

The acceptance for Reaction (1) was determined by simulating events that were evenly distributed over the available phase space. The Monte Carlo events were analyzed by using the exact same reconstruction criteria as the (real) measured data. The same 1C hypothesis was tested in the kinematic fits, and events were selected with the same CL cuts. The acceptance is defined as the ratio of the number of generated to reconstructed Monte Carlo events:

$$A_{\gamma p \rightarrow p X} = \frac{N_{\text{rec,MC}}}{N_{\text{gen,MC}}} \quad (X = \pi^0). \quad (5)$$

In the analysis presented here, we have required the acceptance to be at least 8% in  $(E_\gamma, \theta_{\text{c.m.}})$  bins and removed the other data points from the analysis.

For the extraction of beam asymmetries, it is important to study possible systematic (nonphysics related) contributions to the  $\phi$  distributions. Of particular importance is the influence of the hardware trigger. It required either a hit above a lower-energy threshold in at least two different segments of the TAPS LED-low logical segmentation (Fig. 3, bottom left), or a higher-energy hit

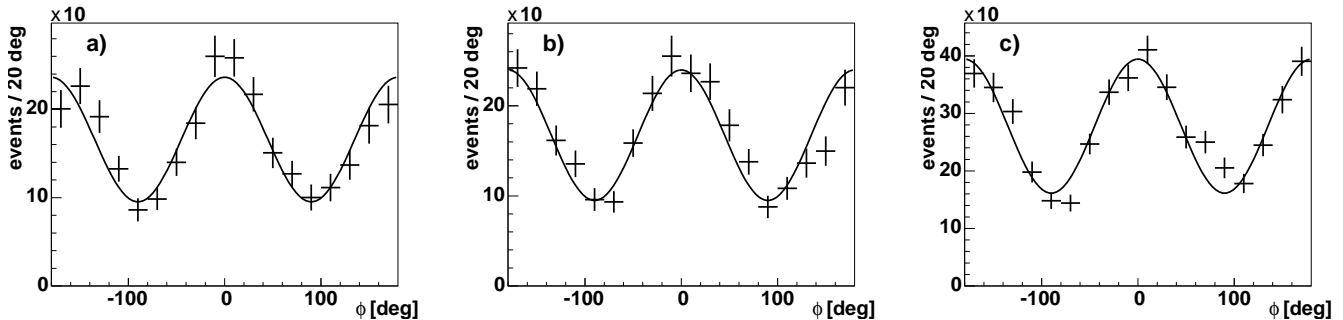


FIG. 7: Typical  $\phi$  distributions for forward-angle bins at  $\theta_{\text{c.m.}} = 35^\circ$  and  $E_\gamma = 1229$  MeV (left), 1295 MeV (middle), and 1625 MeV (right). We have chosen 18 bins in the azimuthal angle  $\phi$ , which corresponds to a bin width of  $20^\circ$ .

in one of the TAPS high-trigger segments (Fig. 3, bottom right) in combination with at least two clusters in the CB was needed (trigger condition 2). If the event kinematics is such that only one particle hits TAPS (possibly leading to condition 2), condition 1 can also be fulfilled simultaneously when the hit occurs close to the edge of a segment. The electromagnetic shower leaking into the adjacent trigger segment then increases the trigger efficiency along the boundaries, imposing a modulation in the  $\phi$  distribution. Figure 6 shows examples of this effect for  $E_\gamma \sim 1560$  MeV. The three peaks are caused by the three boundaries in the logical segmentation of the LED-low trigger. Since this effect is  $\phi$  dependent, it can, in some cases, which depend on event kinematics, significantly contribute to the  $\phi$  modulations. The  $\phi$  distributions in the forward region have, thus, been acceptance corrected to account for the described trigger effect.

## V. EXTRACTION OF $\Sigma$

The polarized cross section in single- $\pi$  photoproduction with linearly polarized photons is proportional to the unpolarized cross section  $(d\sigma/d\Omega)_0$  and is given by

$$\frac{d\sigma}{d\Omega} = \left( \frac{d\sigma}{d\Omega} \right)_0 (1 - P_l \Sigma \cos(2\varphi)), \quad (6)$$

where  $P_l$  denotes the degree of linear beam polarization at an angle  $\varphi$  with respect to the reaction plane, which is spanned by the incoming photon and the recoiling nucleon in the c.m. system. The reaction is schematically shown in Fig. 8. In the experiment, the orientation of the photon polarization is given in the laboratory frame by an angle  $\alpha$  and, thus,  $\varphi = \alpha - \phi$ . For our measurements, the diamond crystal was oriented such that the direction of the beam polarization was perpendicular to the floor of the experimental area ( $\alpha = \pi/2$ ):

$$\frac{d\sigma}{d\Omega} = \left( \frac{d\sigma}{d\Omega} \right)_0 (1 + P_l \Sigma \cos(2\phi)). \quad (7)$$

If the detector setup is invariant with respect to the azimuthal angle, then the observable  $\Sigma$  can be extracted as the amplitude of the  $\phi$  modulation of the  $\pi^0$  meson corrected for the degree of polarization.

Figure 7 shows typical  $\phi$  distributions in the forward region. From fits to these azimuthal event distributions using a function of the form

$$f(\phi) = A + B \cos(2\phi), \quad (8)$$

the product of beam asymmetry and photon polarization  $P_l \Sigma$  is given by the ratio  $B/A$  for each bin of photon energy and  $\pi^0$  polar angle  $\theta_{\text{c.m.}}$ .

### A. Systematic uncertainties

The detection efficiency usually has a weak influence on polarization observables. Most acceptance effects will drop out in the ratio  $B/A$  [Eq. (8)] if the bin sizes are small compared to the variation of the acceptance. Since the extraction of beam asymmetries is based on fits to  $\phi$  distributions, the statistical and systematic errors of  $\Sigma$  cannot easily be separated. For this reason, the error

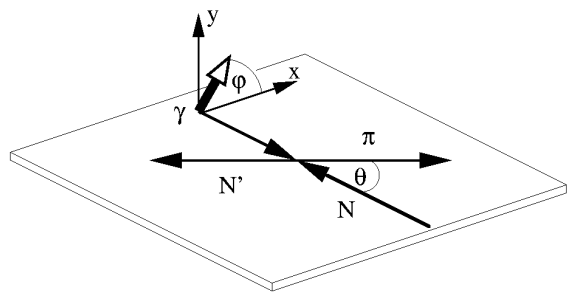


FIG. 8: Sketch of the  $\gamma p \rightarrow p\pi^0$  reaction in the c.m. system; the open (white) arrow indicates the linearly polarized photon.

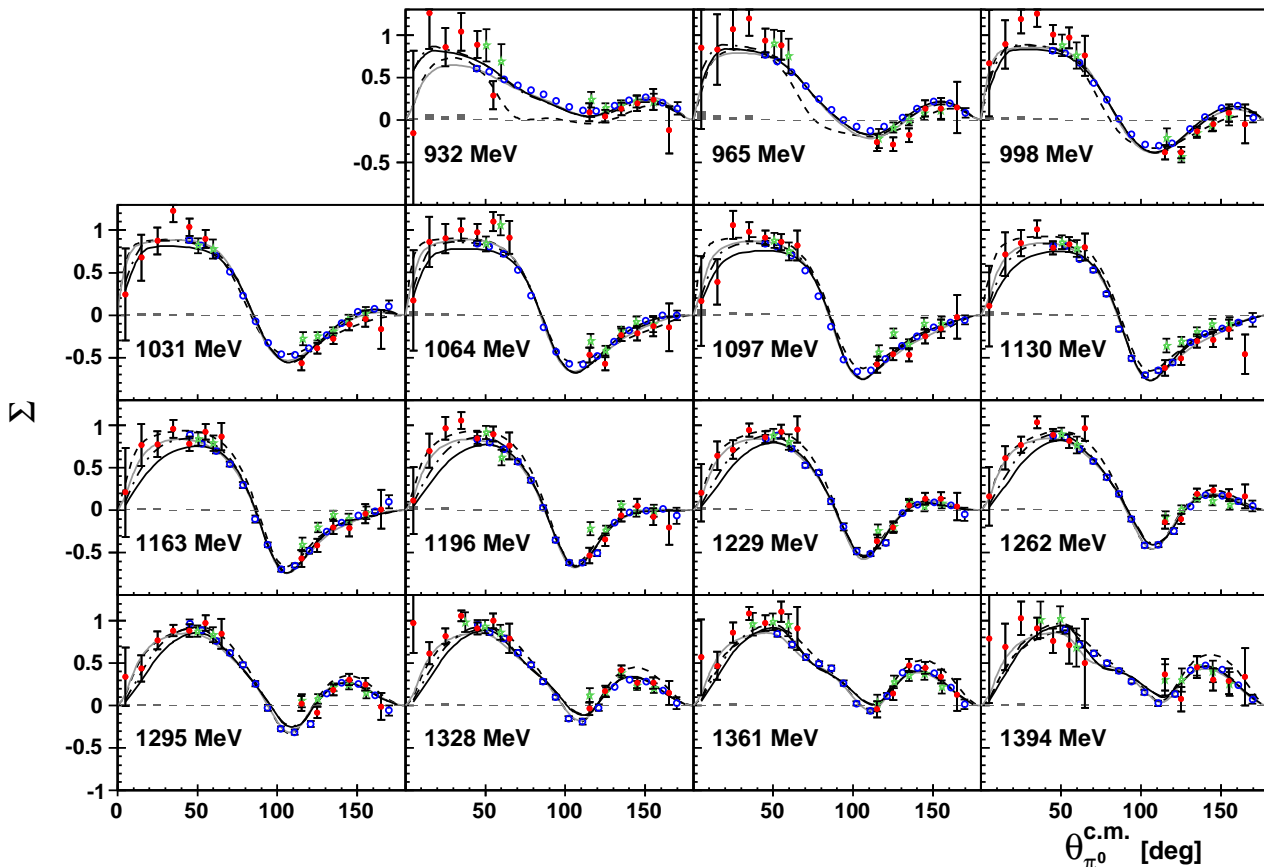


FIG. 9: (Color online) The photon beam asymmetries extracted from the data set with a coherent peak position at 1305 MeV. The filled (red) circles ( $\bullet$ ) denote this analysis, the (green) stars ( $*$ ) denote our previous CBELSA/TAPS analysis [26], and the open (blue) circles ( $\circ$ ) denote the GRAAL results [14]. The black solid line shows the recently published solution of the Bonn-Gatchina partial wave analysis (PWA) [1], the gray solid line denotes the SAID SP09 prediction [18, 44], the dashed black line shows the recent MAID solution [3], and the dashed-dotted line shows a new preliminary solution of the Bonn-Gatchina PWA that includes the results of this analysis [45]. The width of the energy bins is 33 MeV, consistent with the earlier published results. The energy of the bin centers is given in each distribution.

bars (of the data points) in Figs. 9 and 10 consist of both contributions; these errors also include the upper limit on the error of the degree of polarization  $\delta P_\gamma = 0.02$ . Further systematic uncertainties are given separately and are added to the error band.

Systematic errors due to the background subtraction scheme were estimated by performing the following procedure. The beam asymmetries were extracted by using  $\phi$  distributions that have statistical errors determined from the number of events in each bin. In a separate analysis step, the beam asymmetries were found by using  $\phi$  distributions in which the error of each bin is the quadratic sum of the statistical error and the error from the background subtraction. The difference between these results gave an estimate of the systematic error for each data point.

Further contributions to the systematic uncertainties were determined from Monte Carlo studies and acceptance corrections. The reconstruction of neutral pions

and the identification of final states required a sequence of cuts that included the use of kinematic fitting (CL cuts). Error contributions that account for the slightly different effects of CL cuts on data and Monte Carlo events (for the acceptance-corrected forward bins) are estimated at the 3% level, and they are included in the remaining systematic error plotted along the  $\Sigma = 0$  line in each distribution of Figs. 9 and 10.

Additional sources of systematic errors are uncertainties with regard to possible unknown fluctuations of electronic equipment that contribute to the  $\phi$  modulations and a possible offset of the photon beam. While electronic fluctuations have not been studied further, the beam offset was assumed to be shifted by less than 2 mm off axis at the target position. A contribution of such a small offset to the beam asymmetry was found to be negligible.

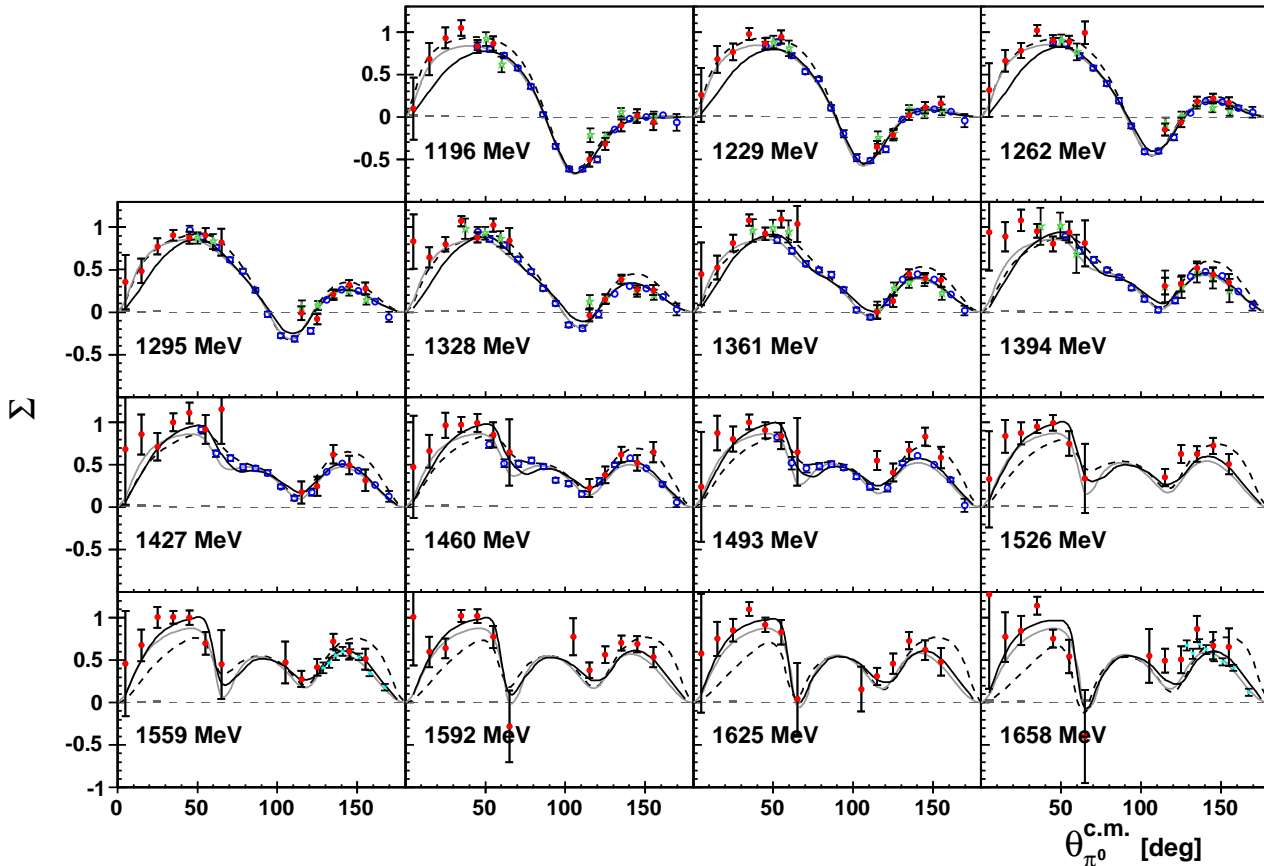


FIG. 10: (Color online) The photon beam asymmetries extracted from the data set with a coherent peak position at 1610 MeV. The filled (red) circles (●) denote this analysis, the (green) stars (★) denote our previous CBELSA/TAPS analysis [26], the open (blue) circles (○) denote the GRAAL results [14], and the (blue-green) stars (★) above 1500 MeV denote recent LEPS results [17]. The black solid line shows the recent solution of the Bonn-Gatchina PWA [1], the gray solid line denotes the SAID SP09 prediction [18, 44], and the dashed black line shows the recent MAID solution [3]. The width of the energy bins is 33 MeV, consistent with the earlier published results. The energy of the bin centers is given in each distribution. For energies below 1400 MeV, we have averaged the results from both data samples.

## VI. EXPERIMENTAL RESULTS

Figure 9 shows the  $\pi^0$  beam asymmetries for our data set with a coherent peak position at 1305 MeV. The unusual energy bin width of 33 MeV was chosen to facilitate the comparison with the GRAAL [14] and the previous CBELSA/TAPS [26] results; small energy shifts among the different data sets are still possible. The data points in the forward region for incoming photon energies below 1 GeV (top row) are statistically limited and have very small degrees of polarization; thus, they have increased error bars. The beam asymmetries for the data set with a coherent peak position at 1610 MeV are shown in Fig. 10 with the same energy binning. For energies above 1400 MeV, the data are extracted from the higher-energy data set alone. In the overlap region between 1200 and 1400 MeV, we have averaged the results from the two data samples (shown in Fig. 10) based on their good

agreement.

The trigger conditions during the “data taking” were not optimized for the production of  $\pi^0$  mesons over the full angular range. For this reason, the  $\Sigma$  distributions exhibit a region of very low acceptance between about  $65^\circ$  and  $115^\circ$ . Our acceptance cut of 8% removes these data points.

The results from this analysis are in excellent agreement with previous measurements. Overall, the new photon beam asymmetries in the forward region and above 1500 MeV also agree nicely with the predictions of the SAID SP09 model [18, 44]. However, small deviations are observed for energies above 1400 MeV, where the broad structure in the forward direction seems to underestimate the data for  $\theta_{c.m.} < 50^\circ$ . The recently published solution of the Bonn-Gatchina PWA [1] is in excellent agreement with the data and SAID over the full range of previously available data, but tends to systematically underestimate the data in the forward region. A new solution

including the results of this analysis is in preparation; the preliminary curve is given by the dashed-dotted line in Fig. 9. Small changes to the width and helicity couplings of the nucleon resonance  $N(1720)P_{13}$  are observed. This is presently being investigated further and will be the subject of a forthcoming publication on *P-wave excited baryons* by the Bonn-Gatchina PWA group [45]. A better understanding of the properties of the  $N(1720)P_{13}$  resonance (from a coupled-channel analysis) will also help resolve its contribution to  $\eta$  photoproduction. Its dominance over contributions from the  $N(1710)P_{11}$  resonance to the reaction  $\gamma p \rightarrow p\eta$  remains disputed.

The MAID 2007 predictions (dashed curves) [3] show overall good agreement with SAID and the experimental data for energies below 1500 MeV. Significant deviations occur in the 932- and 965-MeV photon energy bins for central scattering angles (Fig. 9). At photon energies greater than 1500 MeV, MAID 2007 tends to systematically underestimate the forward region and to overestimate the backward region because (precise) data have been missing. Our new results presented here and the recent LEPS data, which cover the backward region [17], will, thus, be useful to constrain future model solutions and partial wave analyses.

Although it will be possible to modify the model solutions to better describe the data, double-polarization observables are needed to unambiguously extract the scattering amplitude.

## VII. SUMMARY

To summarize, we have presented the results of a re-analysis of previously published CBELSA/TAPS data and new measurements of the beam asymmetry  $\Sigma$  for the photoproduced  $p\pi^0$  final state. New data points have been added to the very forward direction of the  $\pi^0$  meson in the c.m. system. The continuous beam from the ELSA accelerator and the goniometer setup of the experiment provided a linearly polarized tagged-photon beam for the coherent peak positions at 1305 and 1610 MeV. The results are in very good agreement with the earlier measurements at ELSA and also with previous results from other facilities.

## Acknowledgments

We thank all the participating institutions for their invaluable contributions to the success of the experiment. We acknowledge financial support from the National Science Foundation (NSF), Deutsche Forschungsgemeinschaft (DFG) within the SFB/TR16, and from Schweizerischer Nationalfond. The collaboration with St. Petersburg received funds from DFG and the Russian Foundation for Basic Research.

- 
- [1] A. V. Anisovich, E. Klempt, V. A. Nikonov, M. A. Matveev, A. V. Sarantsev and U. Thoma, *Eur. Phys. J. A* **44**, 203 (2010).
  - [2] R. A. Arndt, W. J. Briscoe, I. I. Strakovsky and R. L. Workman, *Phys. Rev. C* **74**, 045205 (2006).
  - [3] D. Drechsel, S. S. Kamalov and L. Tiator, *Eur. Phys. J. A* **34**, 69 (2007).
  - [4] O. Bartholomy *et al.* [CB-ELSA Collaboration], *Phys. Rev. Lett.* **94**, 012003 (2005).
  - [5] M. Yoshioka *et al.*, *Nucl. Phys. B* **168**, 222 (1980).
  - [6] J. C. Bergstrom, R. Igarashi and J. M. Vogt, *Phys. Rev. C* **55**, 2016 (1997).
  - [7] R. Beck *et al.*, *Phys. Rev. Lett.* **65**, 1841 (1990).
  - [8] R. Beck *et al.*, *Phys. Rev. Lett.* **78**, 606 (1997).
  - [9] M. Fuchs *et al.*, *Phys. Lett. B* **368**, 20 (1996).
  - [10] B. Krusche *et al.*, *Eur. Phys. J. A* **6**, 309 (1999).
  - [11] A. Schmidt *et al.*, *Phys. Rev. Lett.* **87**, 232501 (2001).
  - [12] G. Blanpied *et al.*, *Phys. Rev. C* **64**, 025203 (2001).
  - [13] J. Ahrens *et al.* [GDH and A2 Collaborations], *Phys. Rev. Lett.* **88**, 232002 (2002).
  - [14] O. Bartalini *et al.* [GRAAL Collaboration], *Eur. Phys. J. A* **26**, 399 (2005).
  - [15] H. van Pee *et al.* [CB-ELSA Collaboration], *Eur. Phys. J. A* **31**, 61 (2007).
  - [16] M. Dugger *et al.*, *Phys. Rev. C* **76**, 025211 (2007).
  - [17] M. Sumihama *et al.*, *Phys. Lett. B* **657**, 32 (2007).
  - [18] R. A. Arndt, W. J. Briscoe, M. W. Paris, I. I. Strakovsky, and R. L. Workman, Center for Nuclear Studies, Data Analysis Center (DAC): <http://gwdac.phys.gwu.edu/>
  - [19] G. Knies, H. Oberlack, A. Rittenberg, A. H. Rosenfeld, M. Bogdanski, G. Smadja, *Phys. Rev. D* **10**, 2778 (1974).
  - [20] J. Alspector *et al.*, *Phys. Rev. Lett.* **28**, 1403 (1972).
  - [21] P. J. Bussey *et al.*, *Nucl. Phys. B* **104**, 253 (1976).
  - [22] P. J. Bussey *et al.*, *Nucl. Phys. B* **154**, 492 (1979).
  - [23] A. A. Belyaev *et al.*, *Nucl. Phys. B* **213**, 201 (1983).
  - [24] G. Blanpied *et al.* [LEGS Collaboration], *Phys. Rev. Lett.* **69**, 1880 (1992).
  - [25] F. V. Adamian *et al.*, *Phys. Rev. C* **63**, 054606 (2001).
  - [26] D. Elsner *et al.* [CBELSA/TAPS Collaboration], *Eur. Phys. J. A* **39**, 373 (2009).
  - [27] W. Hillert, *Eur. Phys. J. A* **28S1**, 139 (2006).
  - [28] E. Aker *et al.*, *Nucl. Instrum. Meth. A* **321** (1992) 69.
  - [29] A. R. Gabler *et al.*, *Nucl. Instrum. Meth. A* **346**, 168 (1994).
  - [30] R. Novotny [TAPS Collaboration], *IEEE Trans. Nucl. Sci.* **38**, 379 (1991).
  - [31] Daniel Elsner, Ph.D. thesis, University of Bonn, 2007.
  - [32] Frank Klein, Ph.D. thesis (in preparation), University of Bonn; Igor Horn, Ph.D. thesis, University of Bonn, 2004.
  - [33] G. Suft *et al.*, *Nucl. Instrum. Meth. A* **538**, 416 (2005).
  - [34] T. Nakano *et al.*, *Nucl. Phys. A* **684**, 71 (2001).
  - [35] D. Lohmann *et al.*, *Nucl. Instrum. Meth. A* **343**, 494 (1994).
  - [36] K. Livingston, "The Stonehenge Technique. A new method for aligning coherent bremsstrahlung radiators," arXiv:0809.1739 [nucl-ex].
  - [37] F.A. Natter *et al.*, *Nucl. Instrum. Meth. B* **211**, 465 (2003).

- [38] D. Elsner *et al.* [CBELSA/TAPS Collaboration], Eur. Phys. J. A **33**, 147 (2007).
- [39] E. Gutz *et al.* [CBELSA/TAPS Collaboration], Eur. Phys. J. A **35**, 291 (2008).
- [40] F. Klein *et al.* [CBELSA/TAPS Collaboration], Phys. Rev. D **78**, 117101 (2008).
- [41] E. Gutz *et al.* [CBELSA/TAPS Collaboration], Phys. Lett. B **687**, 11 (2010).
- [42] V. Crede *et al.* [CBELSA/TAPS Collaboration], Phys. Rev. C **80**, 055202 (2009).
- [43] M. Williams, M. Bellis and C. A. Meyer, JINST **4**, P10003 (2009).
- [44] M. Dugger *et al.* [CLAS Collaboration], Phys. Rev. C **79**, 065206 (2009).
- [45] A.V. Anisovich, E. Klempt, V.A. Nikonov, A.V. Sarantsev, and U. Thoma (in preparation).